IEEE Access
Multidisciplinary | Rapid Review | Open Access Journal

Received July 17, 2019, accepted August 4, 2019, date of publication August 7, 2019, date of current version August 22, 2019.

Digital Object Identifier 10.1109/ACCESS.2019.2933662

Research on a Novel Flowmeter With Parallel Two-Dimensional Pistons as Its Metering Units

CHUAN DING[1], YUHUI ZHU[1], LI LIU[2], CHENGWEI TONG[1], AND JIAN RUAN[1]

[1]Key Laboratory of Special Purpose Equipment and Advanced Manufacturing Technology, Ministry of Education and Zhejiang Province, Zhejiang University of Technology, Hangzhou 310014, China

[2]School of Engineering, Zhejiang University City College, Hangzhou 310015, China

Corresponding author: Li Liu (miss_liuli@126.com)

This work was supported by the Natural Science Foundation of China under Grant 51805480.

ABSTRACT Flowmeters play a critical role in hydraulic systems. Following a review of positive displacement flowmeters, we hereby introduce a novel positive displacement flowmeter with parallel two-dimensional pistons as metering units. The working principle involves simultaneously utilizing both the rotational and reciprocation movements of a two-dimensional piston and paralleling two two-dimensional pistons to prevent flow rate fluctuations. Consequently, we established a mathematical model to describe the cam track curves and the displacement of the flowmeter. Meanwhile, the pressure loss is analyzed and the leakage flow rate is estimated to compensate the relative error. Finally, we designed and fabricated a prototype to measure the flow rate with ranges of 1 – 25 L/min. The experimental results show that the prototype has a reading uncertainty of less than 2%, a linearity of around ±3.8% and relative errors of less than ±2.9%. The pressure loss for the prototype increases linearly with the total flow rate and reaches 3 bar at 25 L/min. These characteristics are acceptable considering that this prototype is the first set of two-dimensional piston flowmeters. The shortcomings of this first-generation flowmeter are discussed in the conclusion part to provide guidance to enhance the performance of next-generation prototypes.

INDEX TERMS Fluid power, hydraulic system, hydraulic component, flowmeter, two-dimensional piston.

I. INTRODUCTION

Flowmeters are some of the most important instruments both in industrial and scientific applications, because flow rate is a nonnegligible parameter that requires measurement with high accuracy. Though mass flowmeters have been attracting increasing research attention in the last few decades as rapidly developing flowmeters, volumetric flowmeters have steadily maintained its domination in flow measurement [1]. The most critical component in volumetric flowmeters, especially positive displacement flowmeters, is the metering unit, which contains different structures, such as gear, piston, and sliding vane.

Gear flowmeters are considered to have several advantages, such as high accuracy and robustness, high stability, and insensitivity to upstream flow velocity distribution and fluid viscosity [2]. The operating principle involves using a pair of external or internal meshing gears to divide the flow into small counting volumes. The gears, which are normally a pair of external meshing gears, are driven mechanically by the flow. The flow rate is measured by monitoring the rotating speed of the gears. As the most common type used in commercial applications, gear flowmeters have been fully studied and have mature applications for different situations [3]. However, gear flowmeters have drawbacks, such as fluctuations in flow and internal leakage. A planetary gear structure was introduced by Zhang as the metering unit in a flowmeter to reduce fluctuations in the flow rate caused by gear rotation. He compared the external and internal meshing of planetary gear flowmeters and concluded that the latter offers half the flow fluctuation rate of the former [4]. Based on this result, they designed a series of internal meshing planetary gear flowmeters and obtained a minimum flow fluctuation rate that is 1/16 of the normal gear flowmeters [5]. To improve pressure loss and accuracy, several researchers have proposed oval gear flowmeters. Li worked on the meshing characteristic of oval gears, a magnetic sensing distribution plan, and a pair of pressure compensation plate to obtain a high pressure bidirectional oval gear flowmeter [6]. Recently, the oval gear metering unit has also been utilized and reformed by

The associate editor coordinating the review of this manuscript and approving it for publication was Yunjie Yang.

Deng into low eccentricity oval gears to accurately measure tiny flows [7]. In addition, Lukic attempted to further decrease flow fluctuations and pressure loss of oval gear flowmeters by redesigning the inner curve of the metering chamber and interestingly gained a pair of triangle gears as metering units [8].

There are generally two types of piston flowmeters. The motion discipline of the piston in the first one is the reciprocation, which is similar to pistons in a piston pump. The frequency of the reciprocating motion of the piston is monitored and calculated as a flow rate. It is clear that single piston flowmeters exhibit the flow fluctuation phenomenon. Thus, multi-piston flowmeters were invented to minimize fluctuation. Though reciprocating piston flowmeters theoretically have high accuracies due to their face contact sealing zone, the real measuring accuracy depends on the diameter/mass of the pistons. The inertia of pistons leads to vibration under the reciprocating motion, which influences the precision of measurements [9]. Elbretto optimized the inner wall of piston chambers to diminish this vibration [10]. There is another kind of piston flowmeters called oscillating circular piston flowmeters. The meter uses a circular piston in a measuring chamber to form a known volume that momentarily traps liquids from the inlet and discharges them through the outlet side. The flow rate equals the counting number of entrapments in a given period [11]. Recently, Morton published consequent research results on the circular piston flowmeter, including measurement of its liquid film thickness using optical fluorescence [12], experimental analysis of piston movement, pressure loss, leakage flow and abrasion [13], [14], mathematical investigations of forces applied on the piston [11], and two more papers that are yet to be published.

A sliding vane flowmeter divides a known volume by sliding vanes that are evenly distributed in a circumferential direction and measures the flow rate by monitoring the rotating speed. Agustin studied slippage flows caused by pressure drop and established a model for estimating and calibrating meter drifts [15]. Lu et al. proposed a sliding vane flowmeter with combining vanes that can automatically compensate for the gap caused by abrasion [16]. Liu optimized the inner curve of the profiled chamber based on previous research to improve the sealing ability [17].

Various flowmeters have been designed and studied, except the above three kinds. For examples, the roots flowmeter uses a pair of roots to form the counting volume [18], Liu designed a novel flowmeter with a pair of cycloid rotors that has 0.5% accuracy [1], and Herr used two displacement rotors and a blocking rotor to form a flowmeter [19]. The helical screw rotor has also been used to design a new type of flowmeter; it has the advantage of having no flow pulsation and lower pressure loss [20]. However, by classifying positive displacement flowmeters by motion behavior of metering units, it can be used to obtain rotary positive displacement flowmeters and reciprocating positive displacement flowmeters. All these work with one degree of freedom.

The current work emanated from a research group focused on 2D hydraulic components. The concept of ''2D'' implies allowing the critical parts of hydraulic components, such as the spool in servo/proportional valves or the piston in piston pumps, to have two working degrees of freedom. The leader of this group was responsible for inventing a two-dimensional piston mechanism in 2014 and for attempting to redesign hydraulic components based on it [21].

In this work, we present a novel 2D piston flowmeter with parallel two-dimensional pistons as its metering units. The general working principle of the flowmeter is first introduced. Subsequently, we presented the mathematical models, including a description of the piston's motion curve and the cam tracks' curve and the calculation of pressure loss and leakage flow rates. Finally, we fabricated a prototype and performed experiments to estimate the characteristics of the flowmeter.

II. STRUCTURE AND THEORETICAL ANALYSIS

A. GENERAL STRUCTURE

The architecture of a parallel two-dimensional pistons flowmeter is shown in Fig. 1, where the critical components and working spaces are sited. It has two sets of metering units. To simplify reading, the set of metering units composed of components (1) to (6) in Fig. 1 are referred to as the left metering unit, whereas components (9) to (14) are referred to as the right metering unit. Piston (3) with two fixed rollers (1, 6) and piston (12) with two fixed rollers (9, 14) that are the only active parts in the related metering units are considered as piston sets. These two piston sets are solidly combined with each other in the circumferential direction but have independent motions in the axial direction through the combined mechanism of rollers (6) and (9). Two permanent magnets (8) were symmetrically fixed on the combination mechanism of roller (6), implying that a single Hall sensor (7) in the mid-shall can receive two times the signal for each rotation. Besides, it is necessary to introduce the fluid tunnels (B, G). Fluid tunnel (B) connects the left space (A), window (D), and window (I). According to the design in Fig. 1, roller (1) and rollers (6, 9) with the combination mechanism are immersed in the fluid tunnel (B). Fluid tunnel (G) is simply a long tunnel that connects the right space (L), window (E), and window (J), which also contains roller (14).

While highlighting the metering units only, Fig. 2 illustrates the common structure more specifically. Taking the left metering unit (Fig. 2a) as example, the most important components is the piston set which includes the piston (3) and two rollers (1, 6). The piston (3) is precisely contained by the sleeve (4), and two profiled cam tracks (2, 5) are firmly arranged on the two sides of the sleeve (4) and precisely fitted with piston rods (3). Connecting the highest point of the profiled surface to cam track (2) and the lowest point to cam track (5) yields two virtual lines that are parallel to the axis of piston (3) or the x-axis, as shown in Fig. 1, and vice versa. Since roller (1, 6) moves on cam tracks (2, 5), they jointly constitute a motion-converting mechanism from

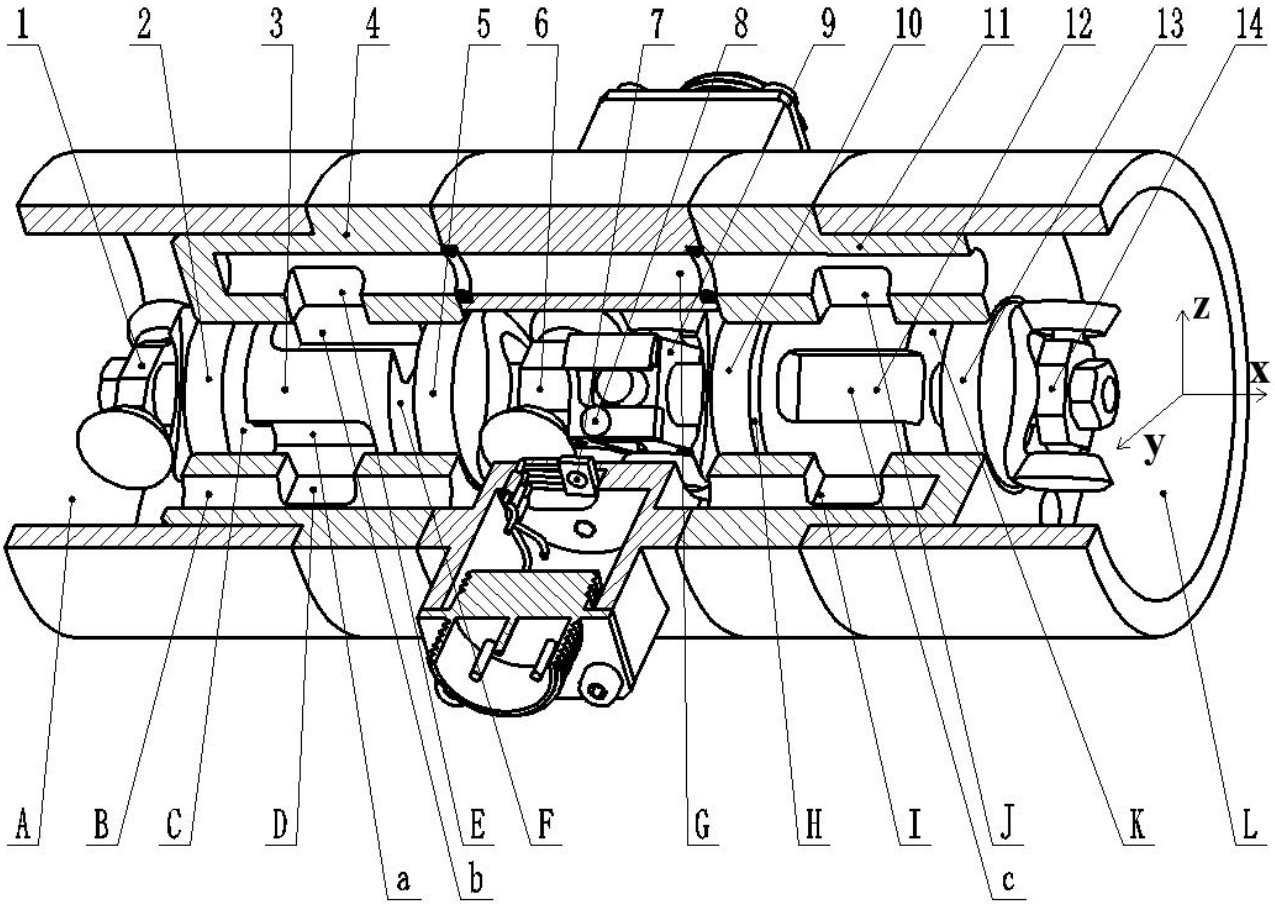

FIGURE 1. General structure of parallel two-dimensional piston flowmeters. 1, 14. Rollers; 2, 5, 10, 13. Cam track; 3, 12. 2D piston; 4. Left sleeve, 6, 9. Roller with combination mechanism; 7. Hall sensors; 8. Permanent magnets; 11. Right sleeve. A. Left space; B, G. Flow tunnel; C, F, H, K. Displacement chamber; D, E, I, J. Window; L. Right space; a, b, c, d. Slot.

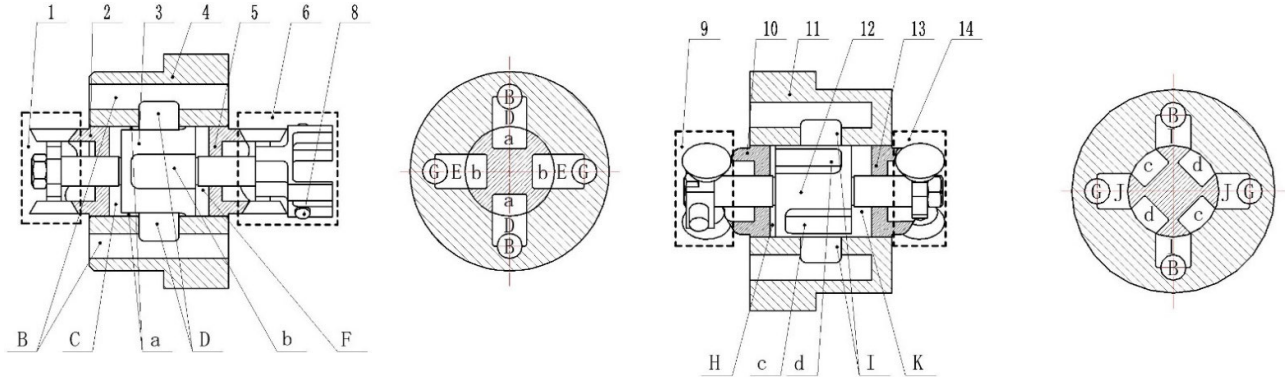

a b

FIGURE 2. Sections of the metering units. a. The left metering unit; b. The right metering unit (all the labels following the same meanings in Fig. 1).

which piston (3) is supported. The displacement chambers (C, F) are formed on the two x-axes of the piston (3) by sleeve (4), piston (3), and two cam tracks (2, 5). There are circumferentially four slots (a, b) that are evenly distributed on piston (3) and alternately connected to the displacement chambers (C, F), i.e., slots (a) are always connected to the displacement chamber (C). On the side of the sleeve (4) and according to slots (a, b), four windows (D, E) are also evenly arranged in the circumferential direction and connected to fluid tunnels (B, G), respectively.

The components and fitting conditions of the right metering unit in Fig. 2b are similar to those on the left metering unit. The major difference between the metering units is that the piston set, including piston (12) and two rollers (9, 14), on the right metering unit has a difference of 45° rotated around the x-axis compared with the piston set on the left metering unit. This difference in angle can theoretically prevent flow fluctuation characteristic for the output flow rate (this is analyzed in Section 3.2) The virtual lines on cam tracks (10, 13) are not only parallel to the x-axis but also coincide with virtual lines on cam tracks (2, 5), implying that unlike two piston groups having angle difference, cam tracks (10, 13) have exactly the same geometrical relationship with cam tracks (2, 5).

B. WORKING PRINCIPLES

The most basic working principle of two-dimensional pistons is simultaneously transferring rotating motion into reciprocating motion, or vice versa. Fig. 3 shows the relationship between the rotating angle and displacement along the x-axis of two pistons, where the states of the pistons in Fig. 1 are assumed as the initial point and the flow comes through the left space (A) first.

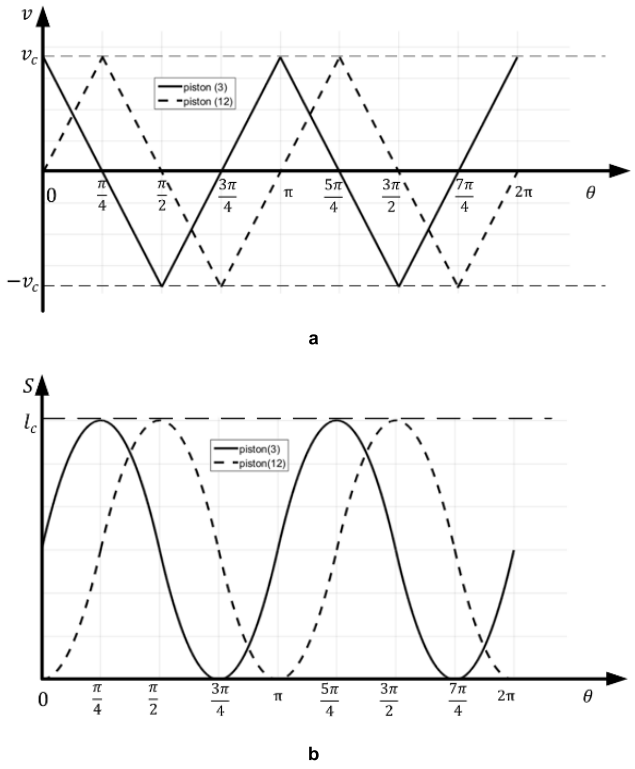

FIGURE 3. The rhythm of pistons' motions. a. The relationship between the rotating angle and x-axial velocities of two pistons. b. The relationship between the rotating angle and x-axial displacements of the two pistons.

Due to the 45° difference and the design of the cam tracks, the curve of piston (12) has a 45° delay than that of piston (3), and the pistons independently reciprocate twice per rotation. The fluid flows alternately through two pistons following the rhythm of motion of the pistons which is shown in Table 1 for clearer illustration.

After the fluid enters into left space (A), it is simultaneously divided into two flows to fulfill windows (D, I) through the fluid tunnel (B). The two situations in Table 1 are described as examples.

Situation 1: at the initial moment in Fig. 1, the rotational angle is assumed to be zero. As illustrated in Fig. 2, the flow areas between window (D) and slot (a) and between window (E) and slot (b) on piston (3) are maximum, whereas the flow areas on piston (12) are closed. The fluid pressure in the displacement chamber (C) forces piston (3) to start to move toward the right and compress the opposite displacement chamber (F) to push out the fluid into the fluid tunnel (G). Meanwhile, piston (3) starts a counterclockwise rotation through the motion-converting mechanism and forces piston (12) to rotate simultaneously through the combination mechanism. Under the assistance of the motion-converting mechanism on the right metering unit, piston (12) moves toward the right to push the fluid in displacement chamber (K) out into fluid tunnel (G). The two flows merge in the right space (L) and leave the flowmeter.

Situation 2: when piston (3) rotates from $\pi/4$ to $\pi/2$, the flow areas between window (D) and slot (b) and between window (E) and slot (a) open. The flow fulfills the displacement chamber (F) to force piston (3) to move toward the left, and the fluid in the displacement chamber (C) is pushed into fluid tunnel (G) through window (E). Due to the combination mechanism, piston (12) also rotates at the same angle. The flow areas between window (I) and slot (d) and between window (J) and slot (c) then close. In this moment, the flow causes the displacement chamber (H) to pull piston (12) to move toward the right.

III. MATHEMATIC MODELS

A. DESCRIPTION OF CAM TRACKS

Since the working principle of this flowmeter is introduced in above section, it is clear that the design of cam tracks is of importance. The two-dimensional pistons are settled parallelly and have 45 degree angle difference between each other when rotating. According to the working principle, the pistons reciprocate twice per rotation and the fluid flows through two pistons alternatively follows the rhythm of pistons' motions. In order to obtain no flow pulsation on the total flow rate passed this flowmeter, a rule of uniform acceleration and deceleration is applied on the design of pistons' motions and the geometry of cam tracks.

Thus, the reciprocating velocities of two pistons are shown in Fig. 3a. Due to the 45 degree angle difference, the dash line of piston (12) has $\pi/4$ delay as the solid line of piston (3). The Fig. 3b demonstrates the relationships between rotation angle and x-axial displacements of pistons, and the solid line of piston (3)'s displacement is also used for designing cam tracks.The set of equation 1 is used to obtain piecewise

TABLE 1. The rhythm rules of the flowmeter for one period ($0 \sim \pi$).

Angle	Tunnel B		Tunnel G		Piston (3)'s position	Piston (12)'s position
	Window (D)'s connection	Window(I)'s connection	Window (E)'s connection	Window(J)'s connection		
0	Slot (a)	Closed	Slot (b)	Closed	mid	Left end
$0\sim\frac{\pi}{4}$	Closing slot (a)	Opening slot (d)	Closing slot (b)	Opening slot (c)	Toward right	Toward right
$\frac{\pi}{4}$	Closed	Slot (d)	Closed	Slot (c)	Right end	mid
$\frac{\pi}{4}\sim\frac{\pi}{2}$	Opening slot (b)	Closing slot (d)	Opening slot (a)	Closing slot (c)	Toward left	Toward right
$\frac{\pi}{2}$	Slot (b)	Closed	Slot (a)	Closed	mid	Right end
$\frac{\pi}{2}\sim\frac{3\pi}{4}$	Closing slot (b)	Opening slot (c)	Closing slot (a)	Opening slot (d)	Toward left	Toward left
$\frac{3\pi}{4}$	Closed	Slot (c)	Closed	Slot (d)	Left end	mid
$\frac{3\pi}{4}\sim\pi$	Opening slot (a)	Closing slot (c)	Opening slot (b)	Closing slot (d)	Toward right	Toward left
π	Slot (a)	Closed	Slot (b)	Closed	mid	Left end

functions for the displacement, velocity and acceleration of pistons from Fig. 3.

$$s = A\theta\left(t\right)^2 + B\theta\left(t\right) + C \tag{1a}$$

$$v = \frac{ds}{dt} = 2A\theta\left(t\right)\frac{d\theta}{dt} + B\frac{d\theta}{dt} \tag{1b}$$

$$a = \frac{dv}{dt} = 2A\left(\left(\frac{d\theta}{dt}\right)^2 + \theta\left(t\right)\frac{d^2\theta}{dt^2}\right) + B\frac{d^2\theta}{dt^2} \tag{1c}$$

where $\theta\left(t\right) = \int_0^t \omega\left(t\right)dt$, $\frac{d\theta}{dt} = \omega\left(t\right)$, $\frac{d^2\theta}{dt^2} = \frac{d\omega}{dt}$. The rotation speed ω depends on the flow rate passing through the flowmeter, which is not predictable for a measuring instrument. For the purpose of simplifying the design process, the rotation speed ω is assumed as a constant value for a constant instantaneous flow rate.

Taking piston (3) as an example, it's easy to obtain $s_{p3} = l_c/2$ when $\theta\left(t\right) = 0$, $s_{p3} = l_c$ when $\theta\left(t\right) = \pi/4$, $s = l_c/2$ when $\theta\left(t\right) = \pi/2$ for piston (3) at $\theta\left(t\right) \in (0, \pi/2)$ in Fig. 3b. Hence, Eq. 2a is used to describe the displacement of piston (3) whereas Eqs. 2b and 2c describe the velocity and acceleration, respectively.

Since piston (12) has 45° difference, the formula for its displacement can be obtained by replacing $\theta\left(t\right)$ in Eq. 2a with $(\theta\left(t\right) - \pi/4)$, as shown in Eq. 3. The results derived for velocity and acceleration are not repeated here.

Hence, the equations to describe the relationship between arc angle, θ, and effective height, h, of the cam track can be obtained using Eq. 2a. A more specific and optimized profile of the cam was presented in [22].

$$\begin{cases} h = -\frac{8l_c}{\pi^2}\theta^2 + \frac{4l_c}{\pi}\theta + \frac{1}{2}l_c & \theta \in \left(0, \frac{\pi}{2}\right) \\ h = \frac{8l_c}{\pi^2}\theta^2 - \frac{12l_c}{\pi}\theta + \frac{9}{2}l_c & \theta \in \left(\frac{\pi}{2}, \pi\right) \\ h = -\frac{8l_c}{\pi^2}\theta^2 + \frac{20l_c}{\pi}\theta - \frac{23}{2}l_c & \theta \in \left(\pi, \frac{3\pi}{2}\right) \\ h = \frac{8l_c}{\pi^2}\theta^2 - \frac{28l_c}{\pi}\theta + \frac{49}{2}l_c & \theta \in \left(\frac{3\pi}{2}, 2\pi\right) \end{cases} \tag{4}$$

B. DISPLACEMENT CALCULATION

In this section, we present the calculation of the displacement for the designed flowmeter based on the working principle and equations of motion of the pistons described above. The basic formula for calculating the instantaneous flow rate passing through the entire flowmeter is as follows, under the assumption that there is no leakage flow.

$$Q_t\left(t\right) = Q_{p3}\left(t\right) + Q_{p12}\left(t\right) \tag{5}$$

Since $Q = \frac{dV}{dt}$, the instantaneous flow rate, $Q_t\left(t\right)$, can be described as

$$Q_t\left(t\right) = \frac{dV_{p3}}{dt} + \frac{dV_{p12}}{dt} = A_p\left(\frac{ds_{p3}}{dt} + \frac{ds_{p12}}{dt}\right) \tag{6}$$

Clearly, the flow rate passing through one metering unit ought to have no negative data because, as mentioned in Section 2.2, displacement chambers are fulfilled with measured liquid and

then push measured liquid out repeatedly. Hence, the instantaneous flow rate follows the next equation

$$Q_t(t) = A_p\left(\left|\frac{ds_{p3}}{dt}\right| + \left|\frac{ds_{p12}}{dt}\right|\right) \tag{7}$$

According to Eqs. 2 and 3, the total flow rate, as shown in Eq. 8, can be described as a constant and can be plotted as shown in Fig. 4, which theoretically has no flow fluctuation.

$$Q_t = \frac{4l_c A_p}{\pi}\omega \tag{8}$$

C. PRESSURE LOSS CALCULATION

It is necessary to assume that the pressure losses occurred in the fluid tunnel and that it was caused by churning motion of the rollers are ignored. The main pressure loss in this flowmeter comes from the throttle loss between the windows and slots and hydraulic resistances to drive all the active parts.

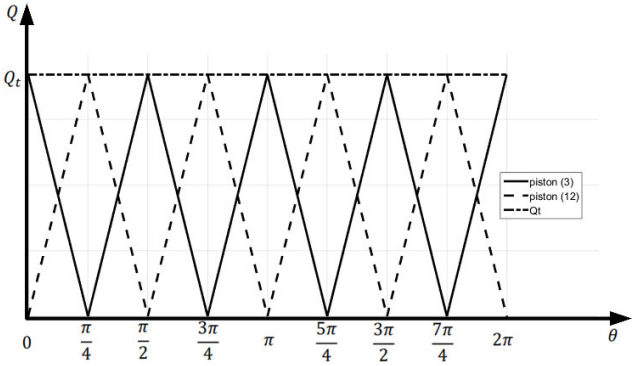

FIGURE 4. Flow rate passing through the flowmeter.

All critical pressure points are plotted in Fig. 5, whereas the initial calculation time is based on Fig. 1.

The throttle loss is directly related to the cross-sectional area and flow rate. According to the design, the flow rate for

$$\begin{cases} s_{p3} = -\frac{8l_c}{\pi^2}\theta(t)^2 + \frac{4l_c}{\pi}\theta(t) + \frac{1}{2}l_c & \theta(t) \in \left(0, \frac{\pi}{2}\right) \\ s_{p3} = \frac{8l_c}{\pi^2}\theta(t)^2 - \frac{12l_c}{\pi}\theta(t) + \frac{9}{2}l_c & \theta(t) \in \left(\frac{\pi}{2}, \pi\right) \\ s_{p3} = -\frac{8l_c}{\pi^2}\theta(t)^2 + \frac{20l_c}{\pi}\theta(t) - \frac{23}{2}l_c & \theta(t) \in \left(\pi, \frac{3\pi}{2}\right) \\ s_{p3} = \frac{8l_c}{\pi^2}\theta(t)^2 - \frac{28l_c}{\pi}\theta(t) + \frac{49}{2}l_c & \theta(t) \in \left(\frac{3\pi}{2}, 2\pi\right) \end{cases} \tag{2a}$$

$$\begin{cases} v_{p3} = -\frac{16l_c}{\pi^2}\omega\theta(t) + \frac{4l_c}{\pi}\omega & \theta(t) \in \left(0, \frac{\pi}{2}\right) \\ v_{p3} = \frac{16l_c}{\pi^2}\omega\theta(t) - \frac{12l_c}{\pi}\omega & \theta(t) \in \left(\frac{\pi}{2}, \pi\right) \\ v_{p3} = -\frac{16l_c}{\pi^2}\omega\theta(t) + \frac{20l_c}{\pi}\omega & \theta(t) \in \left(\pi, \frac{3\pi}{2}\right) \\ v_{p3} = \frac{16l_c}{\pi^2}\omega\theta(t) - \frac{28l_c}{\pi}\omega & \theta(t) \in \left(\frac{3\pi}{2}, 2\pi\right) \end{cases} \tag{2b}$$

$$\begin{cases} a_{p3} = -\frac{16l_c}{\pi^2}\omega^2 & \theta(t) \in \left(0, \frac{\pi}{2}\right) \\ a_{p3} = \frac{16l_c}{\pi^2}\omega^2 & \theta(t) \in \left(\frac{\pi}{2}, \pi\right) \\ a_{p3} = -\frac{16l_c}{\pi^2}\omega^2 & \theta(t) \in \left(\pi, \frac{3\pi}{2}\right) \\ a_{p3} = \frac{16l_c}{\pi^2}\omega^2 & \theta(t) \in \left(\frac{3\pi}{2}, 2\pi\right) \end{cases} \tag{2c}$$

$$\begin{cases} s_{p12} = \frac{8l_c}{\pi^2}\theta(t)^2 & \theta(t) \in \left(0, \frac{\pi}{4}\right) \\ s_{p12} = -\frac{8l_c}{\pi^2}\theta(t)^2 + \frac{8l_c}{\pi}\theta(t) - l_c & \theta(t) \in \left(\frac{\pi}{4}, \frac{3\pi}{4}\right) \\ s_{p12} = \frac{8l_c}{\pi^2}\theta(t)^2 - \frac{16l_c}{\pi}\theta(t) + 8l_c & \theta(t) \in \left(\frac{3\pi}{4}, \frac{5\pi}{4}\right) \\ s_{p12} = -\frac{8l_c}{\pi^2}\theta(t)^2 + \frac{24l_c}{\pi}\theta(t) - 17l_c & \theta(t) \in \left(\frac{5\pi}{4}, \frac{7\pi}{4}\right) \\ s_{p12} = \frac{8l_c}{\pi^2}\theta(t)^2 - \frac{24l_c}{\pi}\theta(t) + 32l_c & \theta(t) \in \left(\frac{7\pi}{4}, 2\pi\right) \end{cases} \tag{3}$$

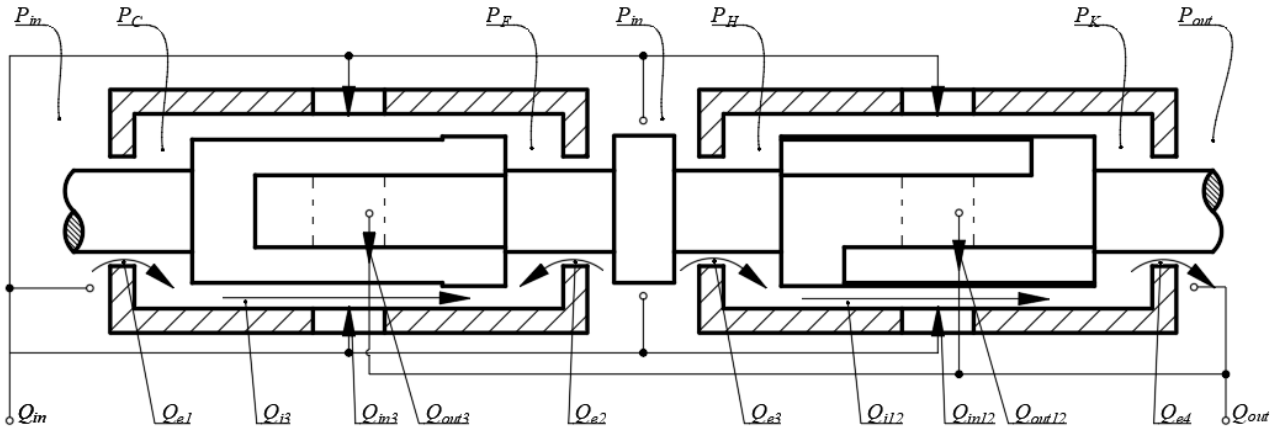

FIGURE 5. Pressure distributions and flow paths of the flowmeter.

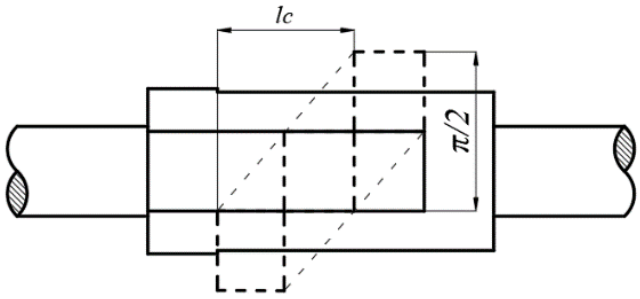

FIGURE 6. The relative position of a window and a slot.

one metering unit simultaneously and evenly passes through two cross-sectional areas that have the same rule of areal changes.

Fig. 6 conceptually illustrates the relative position of a window and a slot when the piston is fixed as a reference. The cross-sectional area is only related to the rotational angle, with an area gradient of $\pi D/8$. Hence, combined with the rhythm of the flow rate distribution shown in Fig. 4, the throttle loss can be derived from the following set of Eq. 9

$$Q_{in3} = 2C_d\left(A_1\sqrt{\frac{2\Delta P_{in-C}}{\rho}} + A_2\sqrt{\frac{2\Delta P_{in-F}}{\rho}}\right) \quad (9a)$$

$$Q_{out3} = 2C_d\left(A_1\sqrt{\frac{2\Delta P_{F-out}}{\rho}} + A_2\sqrt{\frac{2\Delta P_{C-out}}{\rho}}\right) \quad (9b)$$

$$Q_{in12} = 2C_d\left(A_3\sqrt{\frac{2\Delta P_{in-H}}{\rho}} + A_4\sqrt{\frac{2\Delta P_{in-K}}{\rho}}\right) \quad (9c)$$

$$Q_{out12} = 2C_d\left(A_3\sqrt{\frac{2\Delta P_{K-out}}{\rho}} + A_4\sqrt{\frac{2\Delta P_{H-out}}{\rho}}\right) \quad (9d)$$

where C_d is the flow coefficient that has a value of 0.65, where A_1, A_2, A_3, A_4 are the cross-sectional areas between the windows and slots on two pistons and follow the rhythm of Eq. 10, where ΔP is the pressure difference between the two pressure points, indicated by the subscripts of ΔP.

In addition, another part of pressure loss is used to overcome hydraulic resistances. The main resistances discussed here are rolling frictions between the rollers and cam tracks and viscous damping forces between the pistons and sleeves.

To obtain the force of the rolling friction, it is necessary to analyze the force balance and torque balance on each metering unit.

Fig. 7 shows the force balance and torque balance on the piston set on the right metering unit when the rotational angle is $\left(0, \frac{\pi}{4}\right)$. The directions and values of the forces change for different periods of the rotational angle. However, the axial force balance for each metering unit in one period can be obtained using the following general equations.

$$F_{p3} - F_{f3}sin\alpha_3 - F_{N3}cos\alpha_3 - F_{\mu-rec3} = m_{p3}\frac{d^2s_{p3}}{dt^2} \quad (11a)$$

$$F_{p12} - F_{f12}sin\alpha_{12} - F_{N12}cos\alpha_{12} - F_{\mu-rec12} = m_{p12}\frac{d^2s_{p12}}{dt^2} \quad (11b)$$

where F_{px} represents the force provided by the pressure difference; F_{fx} is the rolling friction force; F_{Nx} is the normal force between the roller and the cam track, as illustrated in Fig. 8, $F_{\mu-recx}$ includes the reciprocating viscous damping forces either between the piston and sleeve or between the rods and hubs; and α_x represents the pressure angle. The equations derived for these parameters are listed in Eq. 12.

$$F_{p3} = \Delta P_{C-F} \cdot A_p \quad (12a)$$

$$F_{p12} = \Delta P_{H-K} \cdot A_p \quad (12b)$$

$$F_{fx} = C_r F_{Nx} \quad (12c)$$

$$F_{N3} = F_{RN3}cos\beta \quad (12d)$$

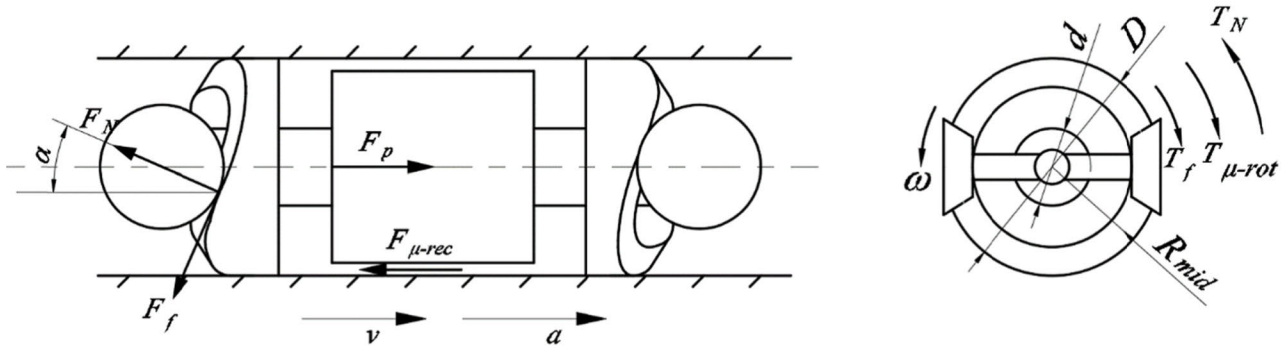

FIGURE 7. The sketch of the force balance and the torque balance on right metering unit when $\theta(t) \in \left(0, \frac{\pi}{4}\right)$.

$$F_{\mu-recx} = \left(\frac{\mu\pi\,(L_1+L_2)\,D}{\delta} + \frac{2\mu\pi L_0 d}{\delta_0}\right) v_{px} \tag{12e}$$

$$\alpha_x = \tan^{-1}\frac{1}{R_{mid}}\frac{ds_{px}}{d\theta} \tag{12f}$$

where $x = 3, 12$ indicates the force on piston (3) or piston (12), β represents the geometrical angle of the rollers, and C_r is the rolling resistance coefficient that has a value of 0.001 in this study. For other periods and for the piston set in the left metering unit, Eqs. 11 and 12 are slightly rewritten. However, the same basic rule applies, and it is not necessary to repeat the entire equations here.

The circumferential torque balance is much more complicated because the two piston sets in the two metering units interact with each other through the combination mechanism on rollers (8, 9). This interaction follows Eq. 13.

$$T_{N3} + T_{N12} = J\frac{d^2\theta}{dt^2} + T_{f3} + T_{f12} + T_{\mu-rot3} + T_{\mu-rot12} \tag{13}$$

where T_{N3} and T_{N12} arise from the normal force, T_{f3} and T_{f12} are caused by rolling friction forces, $T_{\mu-rot3}$ and $T_{\mu-rot12}$ are related to the rotating viscous damping forces

$$\begin{cases} A_1 = \frac{\pi D^2}{8} sin\frac{\pi}{8} - \frac{\pi D^2}{8} sin\frac{\theta}{2} \\ A_2 = 0 \\ A_3 = \frac{\pi D^2}{8} sin\frac{\theta}{2} \\ A_4 = 0 \end{cases} \quad \theta \in \left(0, \frac{\pi}{4}\right) \tag{10a}$$

$$\begin{cases} A_1 = 0 \\ A_2 = \frac{\pi D^2}{8} sin\left(\frac{\theta}{2} - \frac{\pi}{8}\right) \\ A_3 = \frac{\pi D^2}{8} sin\frac{\pi}{8} - \frac{\pi D^2}{8} sin\left(\frac{\theta}{2} - \frac{\pi}{8}\right) \\ A_4 = 0 \end{cases} \quad \theta \in \left(\frac{\pi}{4}, \frac{\pi}{2}\right) \tag{10b}$$

$$\begin{cases} A_1 = 0 \\ A_2 = \frac{\pi D^2}{8} sin\frac{\pi}{8} - \frac{\pi D^2}{8} sin\left(\frac{\theta}{2} - \frac{\pi}{4}\right) \\ A_3 = 0 \\ A_4 = \frac{\pi D^2}{8} sin\left(\frac{\theta}{2} - \frac{\pi}{4}\right) \end{cases} \quad \theta \in \left(\frac{\pi}{2}, \frac{3\pi}{4}\right) \tag{10c}$$

$$\begin{cases} A_1 = \frac{\pi D^2}{8} sin\left(\frac{\theta}{2} - \frac{3\pi}{8}\right) \\ A_2 = 0 \\ A_3 = 0 \\ A_4 = \frac{\pi D^2}{8} sin\frac{\pi}{8} - \frac{\pi D^2}{8} sin\left(\frac{\theta}{2} - \frac{3\pi}{8}\right) \end{cases} \quad \theta \in \left(\frac{3\pi}{4}, \pi\right) \tag{10d}$$

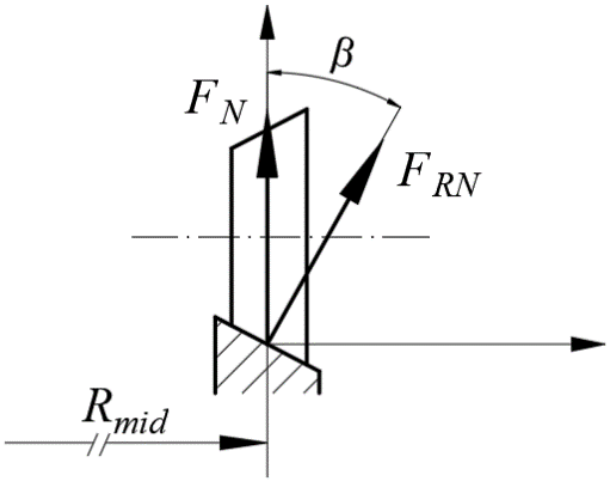

FIGURE 8. Force analysis of a roller.

between the piston and sleeve and between the rods and hubs, and $\frac{d^2\theta}{dt^2} = 0$ for steady flow rate through the flowmeter. The equations derived for these parameters are listed in Eq. 14.

$$T_{Nx} = 2F_{Nx}sin\alpha_x \cdot R_{mid} \tag{14a}$$

$$T_{fx} = 2C_rF_{Nx}cos\alpha_x \cdot R_{mid} \tag{14b}$$

$$T_{\mu-rotx} = \frac{\mu\pi\,(L_1+L_2)\,D^2}{2\delta}\omega \cdot D + \frac{\mu\pi L_0 d^2}{\delta_0}\omega \cdot d \tag{14c}$$

where $x = 3, 12$ indicates the force on piston (3) or piston (12).

Moreover, according to the pressure distribution in Fig. 5 and the parallel structure of the two metering units, the relationship between ΔP_{C-F} and ΔP_{H-K}, which also changes with the rotational angle, can be calculated as follows.

$$\begin{aligned}\Delta P_{C-F} - \Delta P_{H-K} &= (\Delta P_{in-H} - \Delta P_{in-C}) + (\Delta P_{K-out} \\ &\quad - \Delta P_{F-out}) \quad \theta\,(t) \in \left(0, \frac{\pi}{4}\right)\end{aligned} \tag{15a}$$

$$\begin{aligned}\Delta P_{C-F} - \Delta P_{H-K} &= (\Delta P_{in-H} - \Delta P_{in-F}) + (\Delta P_{K-out} \\ &\quad - \Delta P_{C-out}) \quad \theta\,(t) \in \left(\frac{\pi}{4}, \frac{\pi}{2}\right)\end{aligned} \tag{15b}$$

$$\begin{aligned}\Delta P_{C-F} - \Delta P_{H-K} &= (\Delta P_{in-K} - \Delta P_{in-F}) + (\Delta P_{H-out} \\ &\quad - \Delta P_{C-out}) \quad \theta\,(t) \in \left(\frac{\pi}{2}, \frac{3\pi}{4}\right)\end{aligned} \tag{15c}$$

$$\begin{aligned}\Delta P_{C-F} - \Delta P_{H-K} &= (\Delta P_{in-K} - \Delta P_{in-C}) + (\Delta P_{H-out} \\ &\quad - \Delta P_{F-out}) \quad \theta\,(t) \in \left(\frac{3\pi}{4}, \pi\right)\end{aligned} \tag{15d}$$

Finally, by combining Eqs. 9, 11, 13, and 15, an analytical model can be established for pressure distribution in the flowmeter, and its analytical solutions demonstrate the pressure loss due to throttle loss and hydraulic resistances.

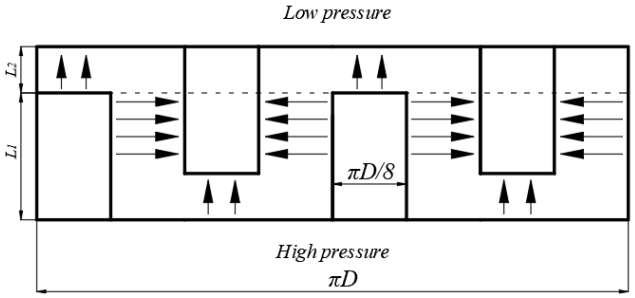

FIGURE 9. The internal leakages of two-dimensional piston.

D. LEAKAGE FLOW RATE CALCULATION

Leakage flow rate exists because of the clearance between the moving and fixed parts and the pressure difference distributed before and after the clearance. One advantage of this flowmeter is that the two-dimensional piston has face sealings instead of the line sealings found in the traditional flowmeters. The leakage paths for this flowmeter are conceptually demonstrated in Fig. 5.

Though all leakages are internal for a flowmeter, there are internal and external leakages for single metering units. The external leakages occurred on the clearances between the rods on pistons and hubs on the sleeves, whereas the internal leakages are due to clearances between the pistons and sleeves. By analyzing the general structures in Section 2.1, it was observed that the directions of the external leakages follow the pressure distribution in the flowmeter. The directions of the internal leakages depend on pressure changes in the displacement chambers.

Generally, together with Eq. 5, the following equation set can be used to describe the flow conditions in the designed flowmeter at steady state.

$$Q_{in} = Q_{in3} + Q_{in12} + Q_{e1} + Q_{e2} + Q_{e3} \tag{16a}$$

$$Q_{out} = Q_{out3} + Q_{out12} + Q_{e4} \tag{16b}$$

$$Q_{in3} + Q_{e1} = Q_{p3} + Q_{i3} = A_p\left|\frac{ds_{p3}}{dt}\right| + Q_{i3} \tag{16c}$$

$$Q_{out3} = Q_{p3} + Q_{i3} + Q_{e2} = A_p\left|\frac{ds_{p3}}{dt}\right| + Q_{i3} + Q_{e2} \tag{16d}$$

$$Q_{in12} + Q_{e3} = Q_{p12} + Q_{i12} = A_p\left|\frac{ds_{p12}}{dt}\right| + Q_{i12} \tag{16e}$$

$$Q_{out12} + Q_{e4} = Q_{p12} + Q_{i12} = A_p\left|\frac{ds_{p12}}{dt}\right| + Q_{i12} \tag{16f}$$

Hence,

$$\begin{aligned}Q_{in} = Q_{out} &= A_p\left|\frac{ds_{p3}}{dt}\right| + A_p\left|\frac{ds_{p12}}{dt}\right| + Q_{i3} + Q_{i12} + Q_{e2} \\ &= Q_t + Q_{i3} + Q_{i12} + Q_{e2}\end{aligned} \tag{17}$$

From Eq. 17, it is clear that the internal leakages have more influence on the accuracy of the flowmeter.

Therefore, we analyze and show the internal leakages for one two-dimensional piston by unfolding the cylinder face of the piston in Fig. 9. It can be divided into two kinds of leakage

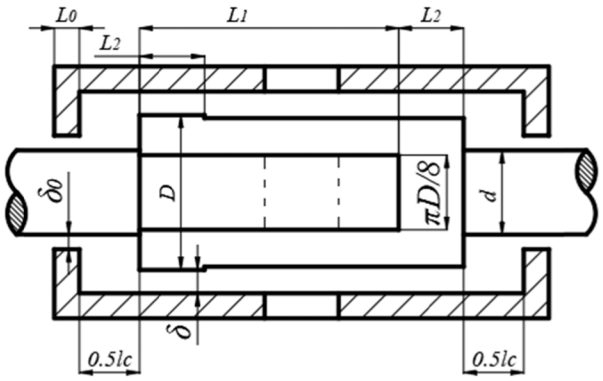

FIGURE 10. The geometry of a piston.

conditions under an assumption of constant gap height. More specifically, the entire sealing area is divided into two parts, as shown in Fig. 9. Two rectangular areas with heights of L_2 and lengths of πD are respectively located at the top and bottom of the sealing area. Since the slots are alternately distributed in these rectangular areas, we combined the two areas into a single rectangular area with no slots, as shown by the area above the dashed line in Fig. 9, to simplify the analysis. In this part, the leakage flow condition comprises flows between two cylindrical concentric walls under a pressure difference and simultaneous reciprocation and rotation of the inner wall. Another part comprises four rectangular areas with heights of $(L_1 - L_2)$ and lengths of $\pi D/8$. Though these four rectangular areas have two different flow directions caused by pressure distribution, they all obey the leakage condition that can be considered as flow between two parallel walls under the condition of that there is a pressure difference and that the lower wall has a moving velocity.

According to the geometry of the piston in Fig. 10, the general evaluation of internal leakages can be derived following the scheme in [23], as presented in Eq. 18.

$$\begin{aligned} Q_{ix} &= \left[\frac{\pi}{6\mu}\cdot\frac{\Delta P_{px}}{L_2}\cdot\frac{1}{2}D\cdot\delta^3+\frac{1}{2}D\pi\delta\cdot v_{px}\right] \\ &\quad +4\left[\frac{1}{12\mu}\cdot\frac{8\Delta P_{px}}{\pi D}\cdot(L_1-L_2)\cdot\delta^3\right] \\ &= K_{ip}\Delta P_{px}+K_{iv}v_{px} \end{aligned} \tag{18}$$

where $x = 3, 12$ differentiates the leakage that occurred in piston (3) to that in piston (12), $K_{ip} = \frac{(\pi^2D^2+32L_2(L_1-L_2))}{12\mu\pi DL_2}\delta^3$, $K_{iv} = \frac{1}{2}\pi D\delta$, $\Delta P_{p3} = \Delta P_{C-F}$, $\Delta P_{p12} = \Delta P_{H-K}$.

Conversely, the external leakage flow rate uses the same formula as the first type of internal leakage and the general evaluation is given as follows.

$$\begin{aligned} Q_{ey} &= \frac{\pi}{6\mu}\cdot\frac{\Delta P_{ey}}{L_0}\cdot\frac{1}{2}d\cdot\delta_0^3+\frac{1}{2}d\pi\delta_0\cdot v_{ey} \\ &= K_{ep}\Delta P_{ey}+K_{ev}v_{ey} \end{aligned} \tag{19}$$

where $y = 1, 2, 3, 4$ is the index number of the external leakage flow shown in Fig. 5, $K_{ep} = \frac{\pi d}{12\mu L_0}\delta_0^3$, $K_{ev} = \frac{1}{2}\pi d\delta_0$, $\Delta P_{e1} = \Delta P_{in-C}$, $\Delta P_{e2} = \Delta P_{in-F}$, $\Delta P_{e3} = \Delta P_{in-H}$, $\Delta P_{e4} = \Delta P_{K-out}$, $v_{e1} = v_{e2} = v_{p3}$, $v_{e3} = v_{e4} = v_{p12}$.

IV. EXPERIMENT RESEARCH

In this section, we report on fabrication of a prototype of the parallel two-dimensional pistons flowmeter, as shown in Fig. 11. The designed measuring range is 1–25 L/min. Specific parameters of the key components are presented in Table 2.

FIGURE 11. The prototype of the parallel two-dimensional pistons flowmeter.

TABLE 2. The parallel two-dimensional pistons flowmeter design.

Name	Value	Unit
Length of slot on piston, L_1	13	mm
Length of sealing face on piston, L_2	2	mm
Length of sealing face on piston rods, L_0	6.4	mm
Length of stroke, l_c	4.2	mm
Diameter of piston, D	18	mm
Diameter of piston rod, d	6	mm
Gap height between piston and sleeve, δ	0.05	mm
Gap height between rod and hub, δ_0	0.03	mm
Geometrical angle of rollers, β	30	°
Total mass of active parts in a metering unit, $m_{p3} = m_{p12}$	0.035	kg

A. EXPERIMENTAL SETUP

As shown in Fig. 12, an experimental setup was developed to test the characteristics of the flowmeter. The entire experimental system comprises a small pump source, which includes an external gear pump with 25 ml/rev displacement, an inverter motor, a 4L accumulator with 0.6 MPa gas precharge pressure and a relief valve with 2 MPa relief pressure, that provides an adjustable but smooth flow rate

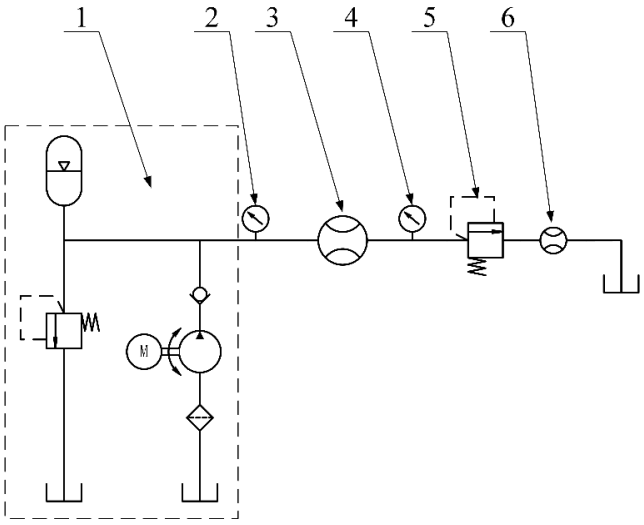

FIGURE 12. The experimental setup. 1. Pump source; 2, 4. pressure sensor; 3. tested flowmeter; 5. loading valve; 6. standard gear flowmeter.

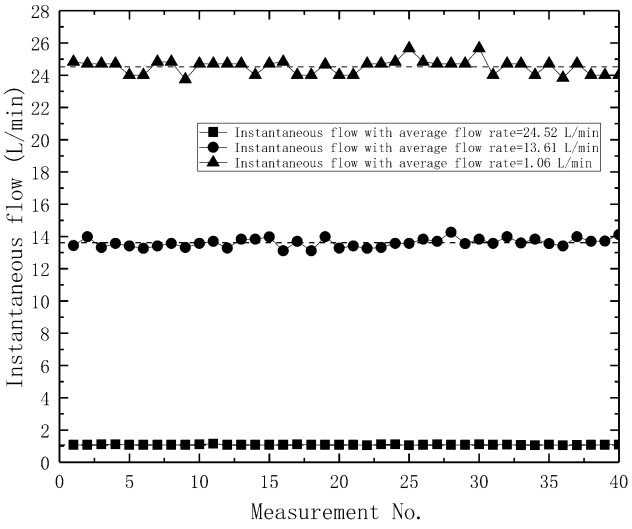

FIGURE 13. Experiments of reading uncertainty.

up to a maximum of 35 L/min, two pressure sensors with 0.5% accuracy, a standard gear flowmeter with a measuring range of 0–40 L/min at 0.3% accuracy, and a loading valve to control the system pressure. The pressure sensors are set to monitor the inlet and outlet pressures of the tested flowmeter. The reading from the standard gear flowmeter is regarded as the true value. Since there is no bypass in this test system, the flow rate passing through the tested flowmeter is exactly the same as that through the standard gear flowmeter. 46# Anti-wear hydraulic oil was applied as a medium in the system, which has 100 cst kinematic viscosity. The compressibility of the hydraulic oil was not considered in this paper due to the low pressure test requirement.

B. RESULTS AND ANALYSIS

1) READING UNCERTAINTY

To obtain the reading uncertainty of this flowmeter, a timer was applied for every four pulses from Hall sensors and set to be triggered by the pulse's rising edge. According to the design of the flowmeter, the fluid displacement during two pulses (one circle) is 5.56 mL/r. Hence, the flow rate through the tested flowmeter was calculated using Eq. 20 as

$$Q_t = \frac{11.12}{\Delta t} \tag{20}$$

where Δt the duration for four pulses recorded by a timer.

This experiment used three constant flow rates (1, 14, 25 L/min), with an inlet pressure of around 1 MPa for the tested flowmeter. Fig. 13 shows 40 measurements for each flow rate and their average values.

According to the test, the reading uncertainty of the parallel two-dimensional pistons flowmeter at all three flow rates is less than 2% at a confidence interval of 95%. This value did not increase with changes in the measured flow rate.

2) DISCHARGE COEFFICIENT AND RELATIVE ERRORS

The discharge coefficient of positive displacement flowmeter that represents the volume of liquid passing through the flowmeter in one output signal pulse can be expressed as Eq. 21.

$$\gamma = \frac{Q}{N_p} \tag{21}$$

where N_p is the number of output signal pulses obtained from the Hall sensors as the pistons rotate one circle. Here $N_p = 2$, due to the number of permanent magnets (8).

Theoretically, the discharge coefficient should be a constant since the structure parameters of a flowmeter are determined by the design. However, it is influenced by the manufacturing, pressure changes in the system, and even the flow rate of the fluid. Since reading from the standard gear flowmeter is taken as the true value, the true discharge coefficient of the true flow rate is expressed here as

$$\gamma_0 = \frac{Q_{in}}{N} = \frac{Q_{out}}{N} \tag{22}$$

where N is the number of pulses output from the Hall sensor, and Q_{in} and Q_{out} represent readings from the standard gear flowmeter. The monitor accounts for the flow rate through the designed displacement by multiplying the output signal pulses in a period. Hence, the theoretical discharge coefficient can be expressed here as

$$\gamma_t = \frac{Q_t}{N} \tag{23}$$

The experiment here is operated under a flow rate of 1 L/min to 31 L/min (20% greater than the design measuring range) and an outlet pressure of 1 MPa that is controlled by the loading valve. The results for both the true discharge coefficient and theoretical discharge coefficient are illustrated in Fig. 14.

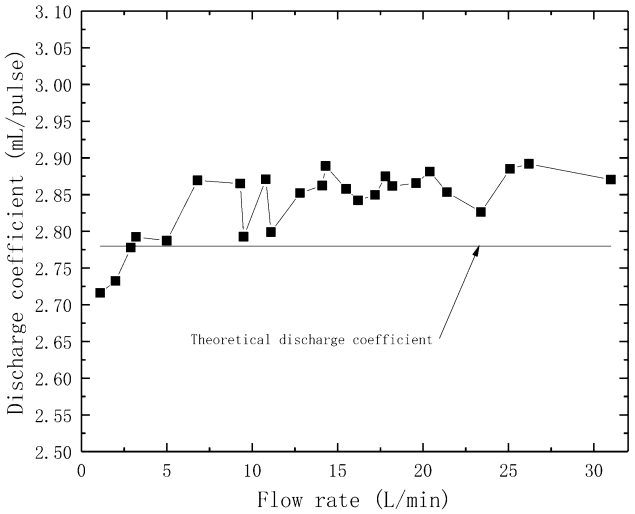

FIGURE 14. Experimental results and theoretical data of the discharge coefficient.

The relative error between these two discharge coefficients ranges from -1.8% up to $+3.9\%$. The internal and external leakages discussed above are undesirable but inevitable. They significantly influence the relative error as a function of geometries of gaps, viscosity, and pressure difference. Therefore, a compensated theoretical discharge coefficient, γ_c based on the theoretical analysis in Section 3 can be obtained through the following relation.

$$\gamma_c = \frac{Q_t + Q_{i3} + Q_{i12} + Q_{e2}}{N} \tag{24}$$

From Fig. 15, the relative error between the compensated discharge coefficients and the experimental results is from -2.9% to $+2.8\%$. Another reason for the error may be the transient internal leakage. Face sealing changes into line sealing at the moment the piston is rotated to a specific angle (as in the right side picture in Fig. 2b). Though the duration of this moment depends on the rotating speed, it still needs to be made as small as possible. Besides leakages, machining errors from fabrication of the prototype can also cause relative errors. There are several mathematical methods for decreasing the relative error, but those are outside the scope of this paper.

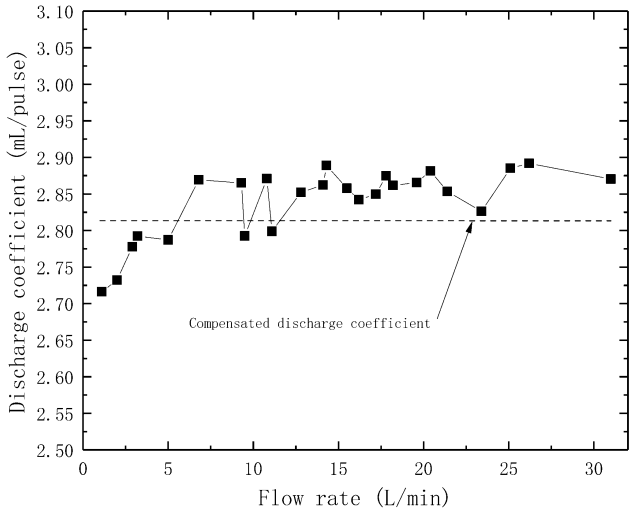

FIGURE 15. Comparing between compensated discharge coefficients and experimental results.

Fig. 16 shows a plot that uses experimental data from the tested flowmeter as the y-axis and true values from a standard gear flowmeter as the x-axis. If there is no error, all the data should be located on the angle bisector. The linearity error of this flowmeter, which is shown more clearly in Fig. 17, is around $\pm 3.8\%$.

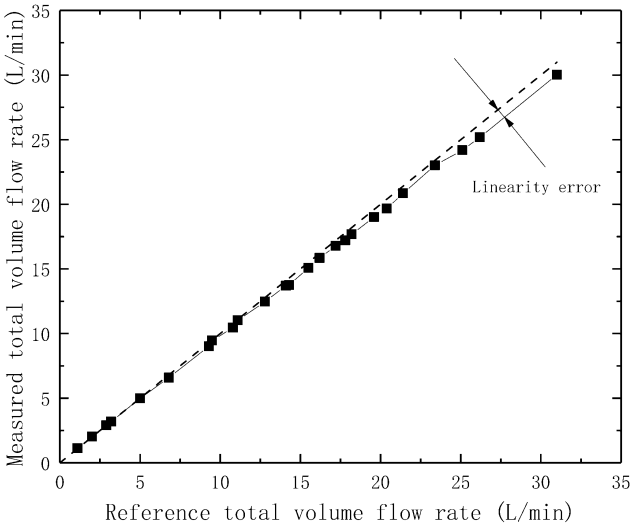

FIGURE 16. Comparison of measurements from two flowmeters.

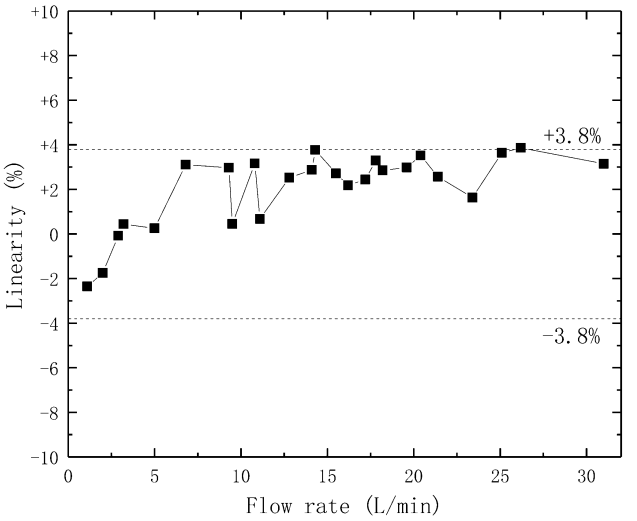

FIGURE 17. The linearity of tested flowmeter.

3) PRESSURE LOSS

Pressure loss is a critical parameter for positive displacement flowmeters that directly affects leakages and energy loss. In this experiment, two high-accuracy pressure sensors

are employed to respectively monitor the inlet and outlet of tested flowmeter. This experiment is operated under the same condition as the experiment in Section 4.2.2. The theoretical pressure difference was analyzed above. Due to the parallel structure, the value of the total pressure difference at the left metering unit should be the same as the value at the right metering unit, as described by Eq. 25.

$$\begin{aligned}\Delta P_{in-out} &= \Delta P_{in-C} + \Delta P_{C-F} + \Delta P_{F-out} \\ &= \Delta P_{in-H} + \Delta P_{H-K} + \Delta P_{K-out} \end{aligned} \quad (25)$$

Both the experimental and calculation results are shown in Fig. 18.

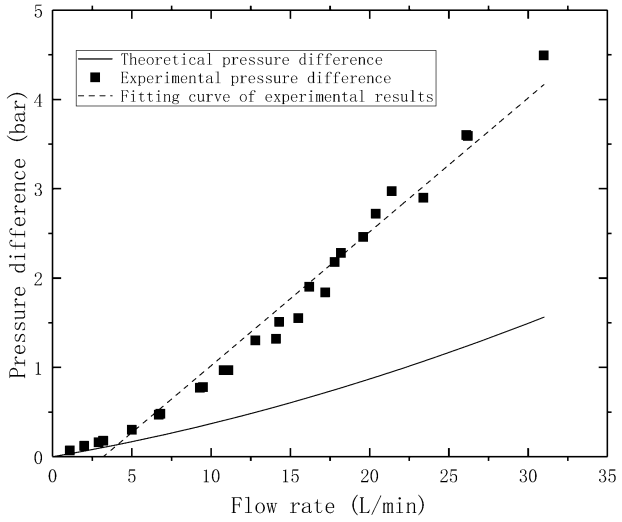

FIGURE 18. Comparison of experimental and theoretical results of pressure difference at tested flowmeter.

The pressure difference of tested flowmeter from the experimental results reaches 4.6 bar for a flow rate of 31 L/min but has a value of less than 3 bar when the flow rate is 25 L/min. However, it is clear that the value of the theoretical pressure difference is less than that of the experimental ones, which might have been due to the neglect of the movement of the rollers in the fluid. In this design, all four sets of rollers were rotating and reciprocating in the fluid tunnel without any form of isolation. They function similar to a single blade pump driven by the pressure difference applied to the working area of the pistons, which directly leads to pressure loss.

V. CONCLUSION AND DISCUSSIONS ON FURTHER RESEARCH

A novel positive displacement flowmeter with parallel two-dimensional pistons as metering units was presented in this paper. Its unique design was founded on simultaneously utilizing both rotation and reciprocation movements of the piston. The working principle involves paralleling two two-dimensional pistons to prevent flow rate fluctuation, as specifically discussed and described in this article. A careful mathematical model was established to describe the cam tracks curves, model the displacement of the flowmeter, and estimate leakage flow rate and pressure loss. Finally, we designed and manufactured a prototype to measure the flow rate in a range of 1–25 L/min under a system pressure of 1 MPa. The experimental results at flow rates of 1, 14, and 25 L/min show that the reading uncertainty of this flowmeter is less than 2%. The full measure range experiment demonstrates a relative error of less than ±2.9% for the prototype after compensation, with a linearity of around ±3.8%. Meanwhile, we observed that the pressure loss increases linearly with the total flow rate, with a value of less than 3 bar at 25 L/min. These results are encouraging, in view of the fact that these are the first set of two-dimensional piston flowmeters. However, for further research, it is necessary to analyze the drawbacks of the flowmeter presented and provide guidance for the design of next-generation flowmeters.

1. The motion-converting and combination mechanisms, including rollers (1, 6, 9, 14) and cam tracks (2, 5, 10, 13), were immersed in the fluid tunnel. The effect of high-speed rotation and reciprocation of rollers in liquid was severely underestimated in designing the flowmeter. This leads to large pressure losses and turbulence in the fluid field, which increases the measuring error. These parts should be isolated from the main fluid tunnel to minimize the effects.

2. The leakage flow rate was greater than expected. As analyzed in Section 3.3, almost all leakages occur in the annular face sealing area; hence, the measuring error should be less than the value obtained for traditional flowmeters. However, the prototype presented a greater measuring error. Though the larger pressure difference should account for this, the transient leakage flow still dominates when the pistons rotate to a specific angle, as shown in Fig. 2b. In this moment, the high pressure side is only sealed by a line from the low pressure side. Considering the processing accuracy during the manufacturing, there is a high possibility for it to become a negative overlapped throttle like the structure in some specially designed valves. A positive overlap structure might be considered in next-generation design, though this would lead to small flow fluctuations.

3. The third problem involves accuracy. The reading uncertainty and linearity were greater than expected, which might have been caused by the permanent magnets used (8). Since they are fixed to the roller (6), the permanent magnets (8) have reciprocating and rotating motions similar to those of the roller (6). This might cause an increase in the reading uncertainty. Hence, the setting of the Hall sensors requires more careful design in the next generation. In addition, the set number of permanent magnets was only 2 in the flowmeter designed and presented here, which is far less than the number used in commercial flowmeters. The accuracy of the next generation of flowmeters will be increased by using more permanent magnets and Hall sensors. Besides, the use of several components in this flowmeter also reduces the measuring accuracy and increases the processing procedures and cost. A simpler structure needs to be explored in the future.

TABLE 3. Table of formulae.

Symbols	Units	Descriptions
$A,\ B,\ C$	[-]	Constant coefficients
A_p	[mm^2]	The working area of a piston, here it is an annulus area, $A_p = \frac{\pi}{4}(D^2 - d^2)$.
$A_1,\ A_2,\ A_3,\ A_4$	[mm^2]	The cross-sectional areas between windows and slots.
$a,\ a_{p3},\ a_{p12}$	[mm/s^2]	Piston's acceleration, the subscripts indicate the piston's number.
C_d	[-]	The flow coefficient, $C_d = 0.65$.
C_r	[-]	The rolling resistance coefficient, $C_r = 0.001$.
D	[mm]	The diameter of pistons
d	[mm]	The diameter of pistons' rods
$F_{p3},\ F_{p12}$	[N]	The hydraulic forces, the subscripts indicate the piston's number.
$F_{f3},\ F_{f12}$	[N]	The rolling friction force between rollers and cam tracks, the subscripts indicate the piston's number.
$F_{N3},\ F_{N12}$	[N]	The normal force between rollers and cam tracks caused by the pressure angle, α, the subscripts indicate the piston's number.
$F_{RN3},\ F_{RN12}$	[N]	The normal force between rollers and cam tracks caused by the geometrical angle of rollers, β, the subscripts indicate the piston's number.
$F_{\mu-rec3},\ F_{\mu-rec12}$	[N]	The reciprocating viscous damping force including the force between piston and sleeve and the force between rods and hubs, the subscripts indicate the piston's number.
h	[mm]	The effective height of cam tracks.
J	[kgm^2]	Moment of inertia.
$K_{ip},\ K_{iv},\ K_{ep},\ K_{ev}$	[-]	The constant coefficients.
$L_0,\ L_1,\ L_2$	[mm]	The geometric parameters on pistons.
l_c	[mm]	The length of stroke.
$m_3,\ m_{12}$	[kg]	The total mass of active parts in a metering unit, the subscripts indicate the piston's number.
N_p	[pulse/min]	The obtained number of output signal pulses from the Hall sensor as pistons rotate one circle.
N	[pulse/min]	The obtained number of output signal pulses from the Hall sensor.
$Q_t,\ Q_{in},\ Q_{out}$	[L/min]	The total flow rate passing the flowmeter, the subscripts indicate the locations where obtain the flow rate.
$Q_{p3},\ Q_{p12}$	[L/min]	The subscripts indicate the flow rate passing the left or right metering unit, while the leakage is neglected.
$Q_{in3},\ Q_{out3},\ Q_{in12},\ Q_{out12}$	[L/min]	The subscripts indicate the flow rate passing the left or right metering unit, while the leakage is considered.
$Q_{e1},\ Q_{e2},\ Q_{e3},\ Q_{e4}$	[L/min]	The external leakage flow rate for the metering units, the subscripts indicate the locations where the external leakages occur.
$Q_{i3},\ Q_{i12}$	[L/min]	The internal leakage flow rate for the metering units, the subscripts indicate the locations where the internal leakages occur.
R_{mid}	[mm]	The radius of cam tracks' mid circle

TABLE 3. *(Continued.)* **Table of formulae.**

$s,\ s_{p3},\ s_{p12}$	[mm]	Piston's displacement, the subscripts indicate the piston's number.
$T_{f3},\ T_{f12}$	[Nm]	The torque caused by the rolling friction force, the subscripts indicate the piston's number.
$T_{N3},\ T_{N12}$	[Nm]	The torque caused by the normal force, the subscripts indicate the piston's number.
$T_{\mu-rot3},\ T_{\mu-rot12}$	[Nm]	The torque caused by rotating viscous damping force, the subscripts indicate the piston's number.
t	[s]	Time.
$V,\ V_{p3},\ V_{p12}$	[mm3]	Volumes of displacement chambers, the subscripts indicate the piston's number.
$v,\ v_{p3},\ v_{p12}$	[mm/s]	Piston's velocity, the subscripts indicate the piston's number.
v_c	[mm/s]	Piston's maximum velocity, $v_c = 4l_c\omega/\pi$.
x	[-]	The index, $x = 3$, or $x = 12$, indicates the piston's number.
y	[-]	The index, $x = 1, 2, 3, 4$, indicates the number of external leakage.
$\Delta P_{in-C},\ \Delta P_{in-F},$ $\Delta P_{C-out},\ \Delta P_{F-out},$ $\Delta P_{in-H},\ \Delta P_{in-K},$ $\Delta P_{H-out},\ \Delta P_{K-out},$ $\Delta P_{C-F},\ \Delta P_{H-K}$	[MPa]	Pressure difference, the subscripts indicate the locations where the internal leakages occur.
$\alpha_{p3},\ \alpha_{p3},\ \alpha_{p12}$	[rad]	The pressure angle of cam track, the subscripts indicate the piston's number.
β	[rad]	The geometrical angle of rollers.
θ	[rad]	Piston's rotation angle.
ω	[rad/s]	Piston's angular velocity.
ρ	[kg/m3]	Density of fluid (hydraulic oil)
δ	[mm]	The designed gap height between piston and sleeve.
δ_0	[mm]	The designed gap height between rod and hub.
$\gamma,\ \gamma_0,\ \gamma_t,\ \gamma_c$	[L/ pulse]	The discharge coefficient, the true discharge coefficient, the theoretical discharge coefficient, the compensated discharge coefficient.

4. The advantage of no flow fluctuation in this flowmeter hasn't been proved experimentally. From equation 8, this flowmeter has theoretically no flow fluctuation phenomenon. However, it's hard to prove it by monitoring the flow fluctuation because there is no such a high frequency flowmeter. Besides, even in the system as Fig. 12, the flow fluctuation caused by the pump source is inevitable. Hence, in the further research, a spectrum analysis based on the pressure data from pressure sensor (2,4) in Fig. 12 would be carried out to explore the flow fluctuation from the flowmeter experimentally. Moreover, it is also possible to introduce the 'Secondary source' method, which is used to measure the pump's flow fluctuation, to investigate the flow fluctuation caused by flowmeters. This area sounds interesting and worth exploring.

Finally, the idea of two-dimensional piston flowmeters is fascinating. The prototype presented in this paper demonstrates the feasibility of this invention. With further research and design and through potential adoption of new manufacturing methods, such as 3D printing, this design of flowmeters would be more mature and very helpful for the development of the next generation of hydraulic components.

REFERENCES

[1] S. Liu, F. Ding, C. Ding, and Z. Man, "A high-pressure bi-directional cycloid rotor flowmeter," *Sensors*, vol. 14, no. 8, pp. 15480–15495, Aug. 2014.
[2] R. C. Baker and M. V. Morris, "Positive-displacement meters for liquids," *Trans. Inst. Meas. Control*, vol. 7, no. 4, pp. 209–220, 1985.
[3] VSE Volumentechnik. (Sep. 22, 2018). *VS Gear Flow Meter*. [Online]. Available: http://www.vse-flow.com
[4] J. Zhang, "The theoretical research on the third planet gear flowmeter for hydraulic system," *Appl. Mech. Mater.*, vol. 20, pp. 407–413, Jan. 2010.
[5] Z. Jun, C. Zhang, Z. Teng, T. Juan, and Z. Bin, "Optimal design of the dynamic gear flowmeter," *Adv. Mater. Res.*, vol. 502, pp. 426–430, Apr. 2012.
[6] B. Li, F. Ding, and Y. Li, "Research on new-type high pressure bi-directional elliptical gear flowmeter," (in Chinese), *Chin. J. Sens. Actuators*, vol. 20, no. 1, pp. 220–223, Jan. 2007.

[7] F. Ding, M. Deng, S. Liu, C. Ding, Z. Man, and Q. Li, "High-pressure bi-directional oval gear tiny-flow meter," (in Chinese), *Trans. Chin. Soc. Agricult. Machinery*, vol. 46, no. 6, pp. 327–333, Jun. 2015.
[8] V. V. Lukic and J. J. Williams, "Porting configuration for a fluid flow meter," U.S. Patent 2016 0 069 721, Mar. 10, 2016.
[9] R. C. Baker, *Flow Measurement Handbook*, 2nd ed. Cambridge, U.K.: Cambridge Univ. Press, 2016.
[10] C. Elbretto and A. White, "Volumetric measuring device with two pistons for a fuel dispensing facility," China Patent 101 750 126 A, Jun. 23, 2010.
[11] C. E. Morton, I. M. Hutchings, J. A. Williams, and R. C. Baker, "Theoretical analysis of the oscillating circular piston positive displacement flowmeter: I—Modelling the forces acting on the piston," *Flow Meas. Instrum.*, vol. 60, pp. 1–16, Apr. 2018.
[12] C. E. Morton, R. C. Baker, and I. M. Hutchings, "Measurement of liquid film thickness by optical fluorescence and its application to an oscillating piston positive displacement flowmeter," *Meas. Sci. Technol.*, vol. 22, no. 12, pp. 125403–125413, Oct. 2011.
[13] C. E. Morton, I. M. Hutchings, and R. C. Baker, "Experimental investigation of an oscillating circular piston positive displacement flowmeter: I—Piston movement and pressure losses," *Flow Meas. Instrum.*, vol. 36, pp. 47–56, Apr. 2014.
[14] C. E. Morton, R. C. Baker, and I. M. Hutchings, "Experimental investigation of an oscillating circular piston positive displacement flowmeter: II—Leakage flows and wear tests," *Flow Meas. Instrum.*, vol. 36, pp. 57–63, Apr. 2014.
[15] A. García-Berrocal, C. Montalvo, J. Blázquez, and M. Balbás, "Flow measurement of liquid hydrocarbons with positive displacement meters: The correction for slippage," *Meas. Sci. Technol.*, vol. 24, no. 5, Apr. 2013, Art. no. 055306.
[16] H. Lei, H. Hu, and Y. Lu, "A dynamic analysis on the transition curve of profiled chamber metering pump," *J. Dyn. Syst., Meas., Control*, vol. 138, no. 7, May 2016, Art. no. 071003.
[17] L. Liu and Y. Lu, "Design of transition curve of profiled chamber flow sensor considering slides with arc ends," *J. Zhejiang Univ.-Sci. A*, vol. 19, no. 2, pp. 137–147, Feb. 2018.
[18] Y.-M. Sun, X.-J. Liu, X.-G. Chen, Q.-Y. Sun, and J. Zhao, "Research and application of a fault self-diagnosis method for roots flowmeter based on WSN node," *Wireless Pers. Commun.*, vol. 95, no. 3, pp. 2315–2330, Apr. 2017.
[19] V. Herr and O. Park, "Rotary positive displacement flowmeter," U.S. Patent 8 100 023 B2, Jan. 24, 2012.
[20] V. B. Kluegl, "Performance prediction model for positive displacement helical screw flowmeters," Ph.D. dissertation, Dept. Mech. Eng., Univ. Glamorgan, Pontypridd, U.K., 1998.
[21] T. Xing, Y. Xu, and J. Ruan, "Two-dimensional piston pump: Principle, design, and testing for aviation fuel pumps," *Chin. J. Aeronaut.*, to be published.
[22] D.-C. Jin, J. Ruan, S. Li, B. Meng, and L.-F. Wang, "Modelling and validation of a roller-cam rail mechanism used in a 2D piston pump," *J. Zhejiang Univ.-Sci. A*, vol. 20, no. 3, pp. 201–217, Mar. 2019.
[23] J. Ivantysyn and M. Ivantysynova, *Hydrostatic Pumps and Motors: Principles, Design, Performance, Modelling, Analysis, Control and Testing*. New Delhi, India: Akademia Books International, 2003.

CHUAN DING received the B.Eng. and Ph.D. degrees in mechatronic control engineering from Zhejiang University, China, in 2008 and 2014, respectively. From 2014 to 2016, he was a Research Fellow with the Institute for Fluid Power Drives and Systems (IFAS), RWTH Aachen University, Germany. He is currently a Lecturer with the School of Mechanical Engineering, Zhejiang University of Technology, China. His research interests include hydraulic components and hydraulic systems.

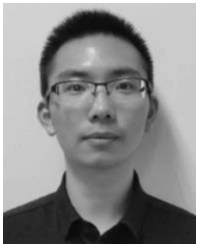

YUHUI ZHU is currently pursuing the degree with the 2D Hydraulic/Pneumatic Components and Systems Engineering Technology Research Center, School of Mechanical Engineering, Zhejiang University of Technology. His research interests include electro-hydraulic control and detection components.

LI LIU received the Ph.D. degree in mechatronic control engineering from Zhejiang University, China, in 2014, where she held a Postdoctoral position at the School of Aeronautics and Astronautics, from 2015 to 2017. She is currently a Lecturer and a Research Fellow with the School of Engineering, Zhejiang University City College, China. Her research interests include engineering mechanics and fluid mechanics.

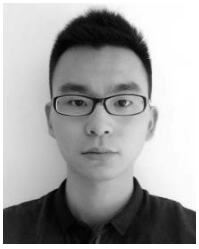

CHENGWEI TONG is currently pursuing the master's degree in mechanical and electrical engineering with the Zhejiang University of Technology. His research interests include electro-hydraulic control and transmission of hydraulic components.

JIAN RUAN received the Ph.D. degree from Harbin Institute of Technology. He is currently a Professor, a Doctoral Tutor, and the Director of the 2D Hydraulic/Pneumatic Components and Systems Engineering Technology Research Center, School of Mechanical Engineering, Zhejiang University of Technology. His research interests include electro-hydraulic digital control systems and components, and electromechanical control technology.